

# Generalized Elliptic Restricted Four-Body Problem with Variable Mass

Abdullah A. Ansari<sup>1\*</sup> and Sada Nand Prasad<sup>2\*\*</sup>

<sup>1</sup>International Center for Advanced Interdisciplinary Research (ICAIR), Sangam Vihar, New Delhi, India

<sup>2</sup>Department of Mathematics Acharya Narendra Dev College, University of Delhi, Delhi, India

Received March 18, 2020; revised March 18, 2020; accepted March 24, 2020

**Abstract**—The elliptic case of restricted four-body problem with variable mass of infinitesimal body is studied here. The three primary bodies which are placed at the vertices of an equilateral triangle and moving in the elliptical orbits around their common center of mass. Out of these primaries we have considered that one massive body is having radiating effect and other two bodies are oblate in shapes. The fourth body which have infinitesimal mass, are varying its mass according to Jeans law. We derive the equations of motion of the infinitesimal body under the generalized sense in the elliptic restricted four-body problem by using the Meshcherskii-space time transformations. Further we numerically study about the equilibrium points, Poincaré surfaces of section, regions of possible motion and basins of the attracting domain by considering the variation of parameters used. Further more we examine the stability of these equilibrium points and found them unstable.

**DOI:** 10.1134/S1063773720040015

**Keywords:** *elliptical orbit, variable mass, oblate, regions of motion, attracting domain.*

## 1. INTRODUCTION

In the present age to write a research article is a serious problem because of the plagiarism. We have to be straight forward towards our aim and goal for the research. Here our field is celestial mechanics and dynamical astronomy which lies in the field of applied mathematics and is branch of mechanics. This study is related to the celestial bodies and behaviour of their motions. During last decades, researchers focused on the study of motion of a small body (in general satellite) under the influence of two, three or four massive bodies but small body is not influencing them. Accordingly they have considered their configurations while these bodies are moving either in circular or elliptical orbits with many other perturbations.

Some of them are as follows: By supposing the bigger primary as oblate spheroid, Sharma and SubbaRao (1976) studied the stationary solutions and their characteristic exponents in the circular restricted 3-body problem. Kalvouridis (1997) investigated the equilibrium points and permissible regions of motion of the minor bodies under the effect of radiated oblate primaries. Douskos (2010) revealed the basins of attraction in the generalized Hill's problem.

Baltagiannis et al. (2011) studied the stability of the equilibrium points of the infinitesimal body

which is moving under the influence of the three primaries. These primaries are situated at the vertices of an equilateral triangle, moving in circular orbits around their common center of mass to which they consider as origin. Further they have studied the zero-velocity surfaces and corresponding equipotential curves. They also found that collinear equilibrium points does not exist when all three-masses are not equal. Furthermore they have illustrated the basins of attraction for the present dynamical model. Kumari and Kushvah (2013, 2014) have illustrated the equilibrium points, their stability, zero-velocity curves as well as the basins of attraction in the restricted four-body problem under the effect of solar drag and oblateness.

Singh and Vincent (2016) studied the motion of infinitesimal body in the generalized restricted three-body problem. Generalized in the sense that both the primaries are radiating, oblate bodies, together with the effect of the gravitational potential from the belt and they found seven equilibrium points instead of five equilibrium points in the classical restricted three-body problem. They also found that collinear points are always unstable while triangular points are stable for some interval of mass ratio. Zotos (2017) performed the basins of attraction in the planar equilateral restricted four-body problem.

Abouelmagd and Ansari (2019) studied numerically the bicircular Sun perturbed Earth-Moon-satellite system and illustrated the equilibrium points,

\*E-mail: [icairndin@gmail.com](mailto:icairndin@gmail.com)

\*\*E-mail: [sadanandprasad@andc.du.ac.in](mailto:sadanandprasad@andc.du.ac.in)

Poincaré surfaces sections and basins of attracting domain. Chakraborty and Narayan (2019a, 2019b) studied the new version of restricted four-body problem when the primaries are moving in elliptical or circular orbits. And illustrated the zero-velocity curves and basins of attraction for the systems.

In general, we suppose that the masses of celestial bodies do not vary with time during the motion. But really many celestial bodies vary their masses with time continuously such as the isotropic radiation or absorption in stars makes their masses variable. Which is an interesting topic in the celestial mechanics and dynamical astronomy, studied by many researchers in the restricted problem (two-body, three-body, four-body and five-body).

Ansari (2017a, 2017b, 2018) and Ansari et al. (2018, 2019a, 2019d) studied the model of restricted problem in three-body, four-body and five-body by considering the variable of mass of the small body. Abouelmagd and Mostafa (2015) investigated the out-of-plane equilibrium points and the regions of possible and forbidden motions of the infinitesimal body which changes the mass according to Jean's law (Jeans 1928) in the frame of restricted three-body problem. Zhang et al. (2012) investigated the triangular equilibrium points in the restricted three-body problem when both the primaries are radiating and infinitesimal body varies its mass according to Jean's law. They used Meshcherskii space time inverse transformation (Meshcherskii 1949) for testing the linear stability of these equilibrium points. Lukyanov (2009) and Singh and Ishwar (1985) investigated the effect of variable mass in the frame of circular restricted three-body problem.

From influencing the previous literatures, we decided to study this problem with equilateral configuration of the primaries with their elliptical motion and variable mass of the small body according to the Jean's law. This article is organised in various sections and subsections which are as follows: The literature review is presented in Section 1. The evaluation of equations of motion are given in Section 2 while Section 3 performed the numerical works with Subsections 3.1, 3.2, 3.3, and 3.4. Section 4 examines the stability of equilibrium points numerically. Finally the paper concluded in Section 5.

## 2. DETERMINATION OF EQUATIONS OF MOTION

Let  $m_1$ ,  $m_2$ ,  $m_3$ , and  $m$  be the masses of three primaries and infinitesimal body, out of which  $m_1$  has the solar radiation pressure ( $q$ ) and  $m_2 = m_3$  have the oblate shapes with oblateness factors  $A_2$  and  $A_3$ , these three bodies are moving in elliptical orbits around their common center of mass which is taken as origin.

In the synodic coordinate system  $xyz$ , the line joining the origin to the primary  $m_1$  is taken as  $x$ -axis while the line perpendicular to this line is considered as  $y$ -axis. The mean motion  $n$  of the system is considered around  $z$ -axis which is perpendicular to the orbital plane of the primaries. The fourth infinitesimal variable mass body is moving under the influence of the primaries while it is not influencing them. It is also assumed that the distances from infinitesimal body to the primaries  $m_1$ ,  $m_2$ , and  $m_3$  are  $r_1$ ,  $r_2$ , and  $r_3$ , respectively. The coordinates of the infinitesimal body and the primaries are  $(x, y, z)$  and  $(x_i, y_i, z_i)$ , ( $i = 1, 2, 3$ ) respectively. Following the procedure given by Ansari et al. (2019c) and Dewangan et al. (2020), we can write the equations of motion of the infinitesimal variable mass body with non-dimensional variables where the variation of mass of the test particle originates from one point and have zero momenta as:

$$\begin{aligned} \frac{\dot{m}}{m}(\dot{x} - y) + (\ddot{x} - 2\dot{y}) &= W_x, \\ \frac{\dot{m}}{m}(\dot{y} + x) + (\ddot{y} + 2\dot{x}) &= W_y, \\ \frac{\dot{m}}{m}\dot{z} + \ddot{z} &= W_z, \end{aligned} \quad (1)$$

where  $(\dot{\phantom{x}})$  denotes the differentiation with respect to  $f$  and  $\frac{df}{dt} = \frac{n(1 + e \cos f)^2}{(1 - e^2)^{3/2}}$ ,

$$\begin{aligned} W &= \frac{1}{n^2(1 + e \cos f)} \left\{ \frac{n^2}{2}(x^2 + y^2 - z^2 e \cos f) \right. \\ &\quad \left. + \frac{(1 - 2\mu)q}{r_1} + \frac{\mu}{r_2} + \frac{\mu A_2}{2r_2^3} + \frac{\mu}{r_3} + \frac{\mu A_3}{2r_3^3} \right\} \end{aligned} \quad (2)$$

with

$$\begin{aligned} r_1^2 &= (x - \sqrt{3}\mu)^2 + y^2 + z^2, \\ r_2^2 &= \left( x + \frac{\sqrt{3}(1 - 2\mu)}{2} \right)^2 + \left( y - \frac{1}{2} \right)^2 + z^2, \\ r_3^2 &= \left( x + \frac{\sqrt{3}(1 - 2\mu)}{2} \right)^2 + \left( y + \frac{1}{2} \right)^2 + z^2, \\ n^2 &= \frac{(1 + e^2)^{3/2}}{a^3(1 - e^2)} \left[ 1 + \frac{3}{2}(A_2 + A_3) \right]. \end{aligned}$$

We will use Jean's law and Meshcherskii space time transformations to preserve the dimension of the space and time as,

$$\begin{aligned} m &= m_0 e^{-\epsilon_1 t}, \quad dt = d\tau, \\ x &= \epsilon_2^{-1/2} \alpha, \quad \dot{x} = \epsilon_2^{-1/2} \left( \dot{\alpha} + \frac{\epsilon_1}{2\epsilon_3} \alpha \right), \end{aligned}$$

$$\begin{aligned} \ddot{x} &= \epsilon_2^{-1/2} \left( \ddot{\alpha} + \frac{\epsilon_1}{\epsilon_3} \dot{\alpha} + \frac{(\epsilon_1^2 - 2\epsilon_1\epsilon_4)}{4\epsilon_3} \alpha \right), \\ y &= \epsilon_2^{-1/2} \beta, \quad \dot{y} = \epsilon_2^{-1/2} \left( \dot{\beta} + \frac{\epsilon_1}{2\epsilon_3} \beta \right), \\ \ddot{y} &= \epsilon_2^{-1/2} \left( \ddot{\beta} + \frac{\epsilon_1}{\epsilon_3} \dot{\beta} + \frac{(\epsilon_1^2 - 2\epsilon_1\epsilon_4)}{4\epsilon_3} \beta \right), \\ z &= \epsilon_2^{-1/2} \gamma, \quad \dot{z} = \epsilon_2^{-1/2} \left( \dot{\gamma} + \frac{\epsilon_1}{2\epsilon_3} \gamma \right), \\ \ddot{z} &= \epsilon_2^{-1/2} \left( \ddot{\gamma} + \frac{\epsilon_1}{\epsilon_3} \dot{\gamma} + \frac{(\epsilon_1^2 - 2\epsilon_1\epsilon_4)}{4\epsilon_3} \gamma \right), \end{aligned} \quad (3)$$

where  $\epsilon_1$  is constant coefficient,  $\epsilon_2 = \frac{m}{m_0}$ ,  $\epsilon_3 = \frac{df}{dt}$ ,  $\epsilon_4 = \frac{d^2f}{dt^2}$  and  $m_0$  is the initial mass.

After using Eq. (3) in the Eq. (1), we get

$$\begin{aligned} \ddot{\alpha} - 2\dot{\beta} &= \frac{\partial U}{\partial \alpha}, \\ \ddot{\beta} + 2\dot{\alpha} &= \frac{\partial U}{\partial \beta}, \\ \ddot{\gamma} &= \frac{\partial U}{\partial \gamma}, \end{aligned} \quad (4)$$

where

$$\begin{aligned} U &= \frac{1}{(1 + e \cos f)} \left[ \left\{ \frac{\epsilon_5}{8} (\alpha^2 + \beta^2 + \gamma^2) \right. \right. \\ &+ \left. \frac{1}{2} (\alpha^2 + \beta^2 - \gamma^2 e \cos f) \right\} + \frac{\epsilon_2^{3/2}}{n^2} \left\{ \frac{(1 - 2\mu)q}{\rho_1} \right. \\ &\left. \left. + \frac{\mu}{\rho_2} + \frac{\mu A_2 \epsilon_2}{2\rho_2^3} + \frac{\mu}{\rho_3} + \frac{\mu A_3 \epsilon_2}{2\rho_3^3} \right\} \right] \end{aligned} \quad (5)$$

with

$$\begin{aligned} \epsilon_5 &= \frac{4\epsilon_1\epsilon_4 + \epsilon_1^2}{4\epsilon_3^2} \\ \rho_1^2 &= (\alpha - \sqrt{3\epsilon_2}\mu)^2 + \beta^2 + \gamma^2, \\ \rho_2^2 &= \left( \alpha + \frac{\sqrt{3\epsilon_2}(1 - 2\mu)}{2} \right)^2 \\ &+ \left( \beta - \frac{\sqrt{\epsilon_2}}{2} \right)^2 + \gamma^2, \\ \rho_3^2 &= \left( \alpha + \frac{\sqrt{3\epsilon_2}(1 - 2\mu)}{2} \right)^2 \\ &+ \left( \beta + \frac{\sqrt{\epsilon_2}}{2} \right)^2 + \gamma^2. \end{aligned} \quad (6)$$

Initially i.e.,  $t = 0$  and  $f = f_0$ , the Jacobian can be written as

$$\dot{\alpha}^2 + \dot{\beta}^2 + \dot{\gamma}^2 = 2U - C, \quad (7)$$

where left hand side of Eq. (7) represents the velocity of the infinitesimal body and  $C$  is the conserved Jacobian constant for the system. The regions of motion are restricted for the given values of energy, where it can move i.e.,  $2U \geq C$ , and all other places are prohibited. In general shaded regions are the prohibited regions.

### 3. NUMERICAL STUDIES

#### 3.1. Positions of Equilibrium Points

Positions of equilibrium points can be obtained in  $\alpha-\beta$ -plane after solving the right hand sides of the system (4), i.e.,  $U_\alpha = 0$  and  $U_\beta = 0$ , and hence

$$\begin{aligned} \alpha \left( 1 + \frac{\epsilon_5}{4} \right) - \frac{\epsilon_2^{3/2}}{n^2} \left\{ \frac{q(1 - 2\mu)(\alpha - \sqrt{3\epsilon_2}\mu)}{\rho_1^3} \right. \\ + \frac{\mu(\alpha + \sqrt{3\epsilon_2}(1 - 2\mu)/2)}{\rho_2^3} \\ + \frac{3A_2\epsilon_2\mu(\alpha + \sqrt{3\epsilon_2}(1 - 2\mu)/2)}{2\rho_2^5} \\ + \frac{\mu(\alpha + \sqrt{3\epsilon_2}(1 - 2\mu)/2)}{\rho_3^3} \\ \left. + \frac{3A_3\epsilon_2\mu(\alpha + \sqrt{3\epsilon_2}(1 - 2\mu)/2)}{2\rho_3^5} \right\} = 0, \end{aligned} \quad (8)$$

$$\begin{aligned} \beta \left( 1 + \frac{\epsilon_5}{4} \right) - \frac{\epsilon_2^{3/2}}{n^2} \left\{ \frac{q(1 - 2\mu)\beta}{\rho_1^3} + \frac{\mu(\beta - \sqrt{\epsilon_2}/2)}{\rho_2^3} \right. \\ + \frac{3A_2\epsilon_2\mu(\beta - \sqrt{\epsilon_2}/2)}{2\rho_2^5} + \frac{\mu(\beta + \sqrt{\epsilon_2}/2)}{\rho_3^3} \\ \left. + \frac{3A_3\epsilon_2\mu(\beta + \sqrt{\epsilon_2}/2)}{2\rho_3^5} \right\} = 0. \end{aligned} \quad (9)$$

After numerically solving Eqs. (8) and (9) for the variations of the parameters used with the help of well known software Mathematica, we perform these graphs in Figs. 1–3. Figure 1 represents the variation of the value in eccentricity  $e$  (0.15 (Fig. 1a), 0.35 (Fig. 1b), 0.65 (Fig. 1c)). Figures 1a–1c present eight, eight, and four equilibrium points with black, blue, and red dots, respectively. From these figures, we observed that as increasing the value of  $e$ , some equilibrium points are extinct (as in Fig. 1c), equilibrium points  $L_5, L_6, L_7$ , and  $L_8$  are not present. In this way  $e$  has the reduction effect.

Figure 2 shows the variation of variation parameter  $\epsilon_2$  (0.4 (Fig. 2a), 0.8 (Fig. 2b), 1.2 (Fig. 2c)). Figure 2d shows the combination of the Figs. 2a–2c). From Fig. 2 we noted that as increasing the value of  $\epsilon_2$  all the equilibrium points are moving away. Therefore  $\epsilon_2$  has expanding effect.

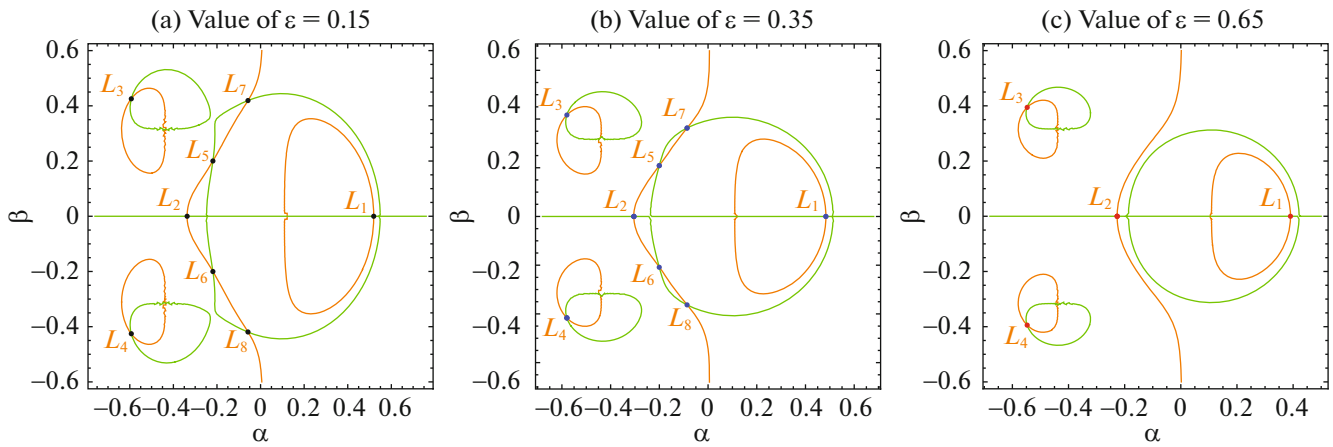


Fig. 1. Positions of equilibrium points in  $\alpha$ - $\beta$ -plane at  $\epsilon_1 = 0.2$ ,  $f = 0$ ,  $a = 0.75$ ,  $\epsilon_2 = 0.4$ ,  $\mu = 0.1$ ,  $q = 0.9$ ,  $A_2 = A_3 = 0.05$ .

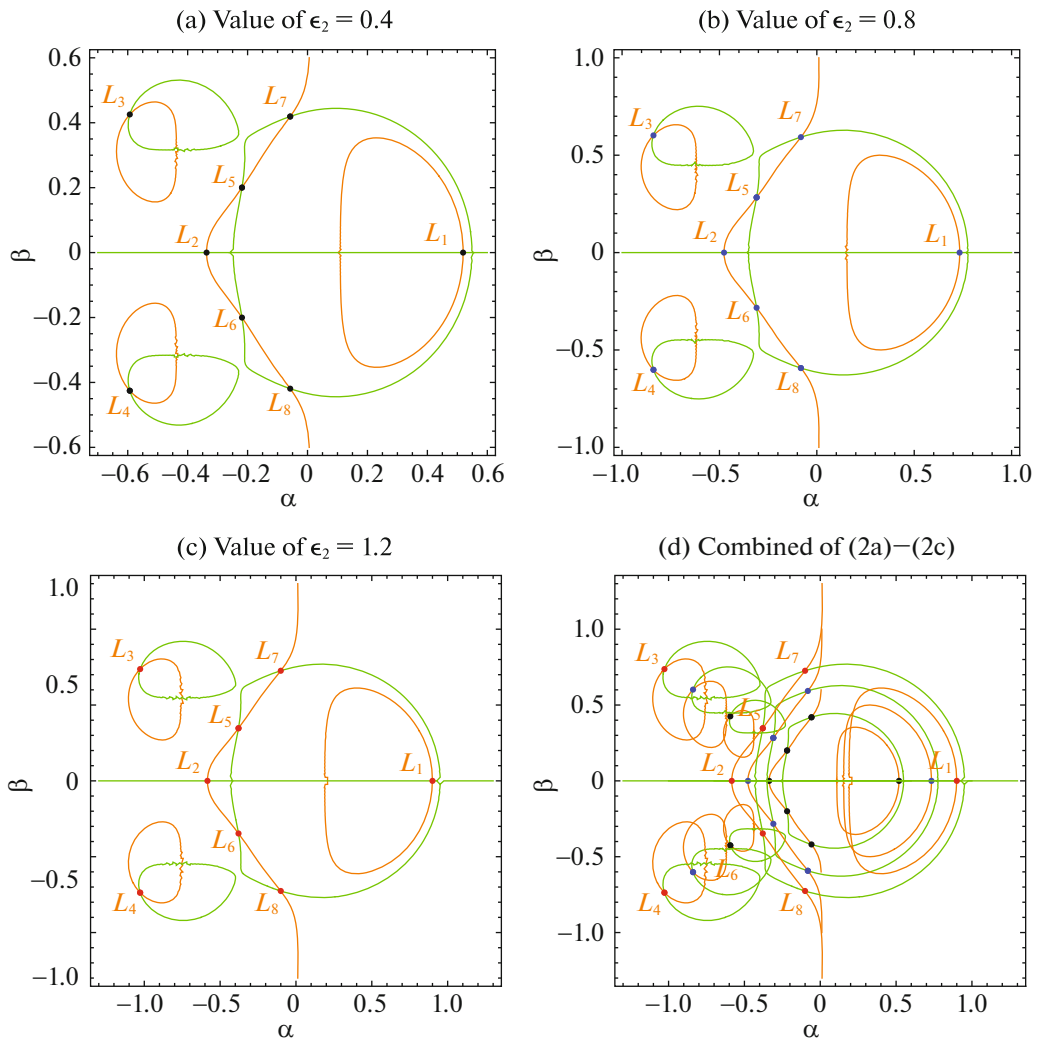


Fig. 2. Positions of equilibrium points in  $\alpha$ - $\beta$ -plane at  $\epsilon_1 = 0.2$ ,  $e = 0.15$ ,  $f = 0$ ,  $a = 0.75$ ,  $\mu = 0.1$ ,  $q = 0.9$ ,  $A_2 = A_3 = 0.05$ .

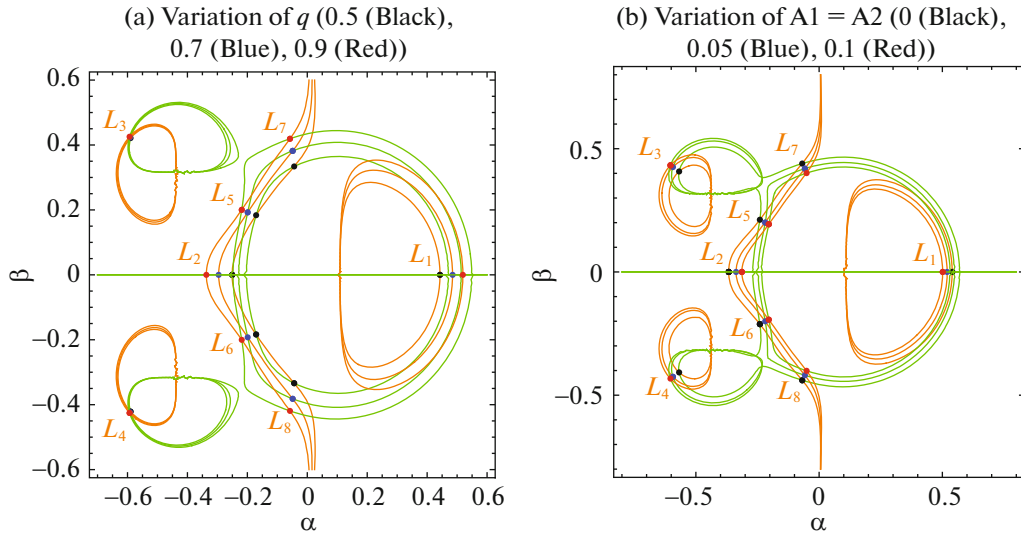


Fig. 3. Positions of equilibrium points in  $\alpha$ - $\beta$ -plane at  $\epsilon_1 = 0.2$ ,  $f = 0$ ,  $a = 0.75$ ,  $\epsilon_2 = 0.4$ ,  $\mu = 0.1$ .

Figure 3 presents the variations of solar radiation pressure  $q$  (0.5 (Black), 0.7 (Blue), 0.9 (Red) (Fig. 3a)) and oblateness of the primaries (0 (Black), 0.05 (Blue), 0.1 (Red) (Fig. 3b)). From Fig. 3a, we pointed out that increasing the value of  $q$ , the equilibrium points  $L_3$  and  $L_4$  are unchanged in their positions while all other six equilibrium points  $L_1$ ,  $L_2$ ,  $L_5$ ,  $L_6$ ,  $L_7$ , and  $L_8$  are moving away from their previous positions. From Fig. 3b, we found that as we increase the value of oblateness, the equilibrium points  $L_3$  and  $L_4$  are moving away while all other six equilibrium points  $L_1$ ,  $L_2$ ,  $L_5$ ,  $L_6$ ,  $L_7$ , and  $L_8$  are moving towards the origin. In this way, solar radiation factor has expanding effect while oblateness has both expanding and shrinking effects.

### 3.2. Poincaré Surfaces of Section

To examine the chaotic or regular behavior of the path of the test particle, we have to plot the Poincaré surfaces of section. For which we must find the position and velocity of the infinitesimal body in phase space. The graph between  $\alpha$  and  $\alpha'$  (differentiation with respect to time  $t$ ) should be plotted when  $\beta = 0$ , whenever the orbit intersects the plane at  $\beta' \geq 0$ . Here plotted the Poincaré surfaces of section and given in Figs. 4–7. We observed from Fig. 4 that as increase the value of  $\epsilon_2$ , the surfaces of section changes into more and more regular and smooth. Figure 5 represent the Poincaré surfaces of section the variation of true anomaly ( $f = 0, \pi/6, \pi/3, \pi/2, \pi$ , and  $3\pi/2$ ) with constant mass (i.e.,  $\epsilon_1 = 0$  and  $\epsilon_2 = 1$ ). From Figs. 4–7 we observed that there are no chaos i.e., smooth for  $f = 0, \pi/6, \pi/3, \pi/2, \pi$  but for  $f = 3\pi/2$ , there is zigzag surfaces which is chaos. Figure 6 represent

the Poincaré surfaces of section with the variation of true anomaly ( $f = 0, \pi/6, \pi/3, \pi/2, \pi$ , and  $3\pi/2$ ) with variable mass (i.e.,  $\epsilon_1 = 0.2$  and  $\epsilon_2 = 0.4$ ). From these figures we noted that all surfaces are smooth except for  $f = 3\pi/2$  where chaos is appear. Figure 7 represent the Poincaré surfaces of section with the variation of eccentricity ( $e = 0.15, 0.35$ , and  $0.65$ ) with variable mass (i.e.,  $\epsilon_1 = 0.2$  and  $\epsilon_2 = 0.4$ ). From these figures we observed that as increase the value of  $e$  the smoothness of the curves reduces. In this way the parameters used have excellent effect on Poincaré surfaces of section.

### 3.3. Regions of Possible Motion

To reveal the regions of possible or forbidden motion, we follow the procedure and terminology used by Ansari et al. (2019b) and Dewangan et al. (2020). Accordingly, we have determined the each value of Jacobian constant corresponding to the each equilibrium point and then drawn the regions of forbidden motion with the help of Eq. (7) and performed purple shaded regions as the forbidden regions which are shown in Fig. 8. This figure suggests very important dynamical properties of the motion of the infinitesimal body. Figure 8a represents the region corresponding to the equilibrium point  $L_1$  and shows that infinitesimal body can move near all the primaries except the purple color shaded region i.e., it can not move near  $L_2$ ,  $L_5$ ,  $L_6$ ,  $L_7$ , and  $L_8$ . It can move freely around  $m_2$  and  $m_3$  while around  $m_1$ , it can move only in circular region by entering from  $L_1$  which is a gateway for the circular region. Figure 8b represents the region corresponding to the equilibrium points  $L_2$  and shows that the small particle can move freely except near the equilibrium points  $L_7$ ,  $L_8$ . Figure 8c represents the

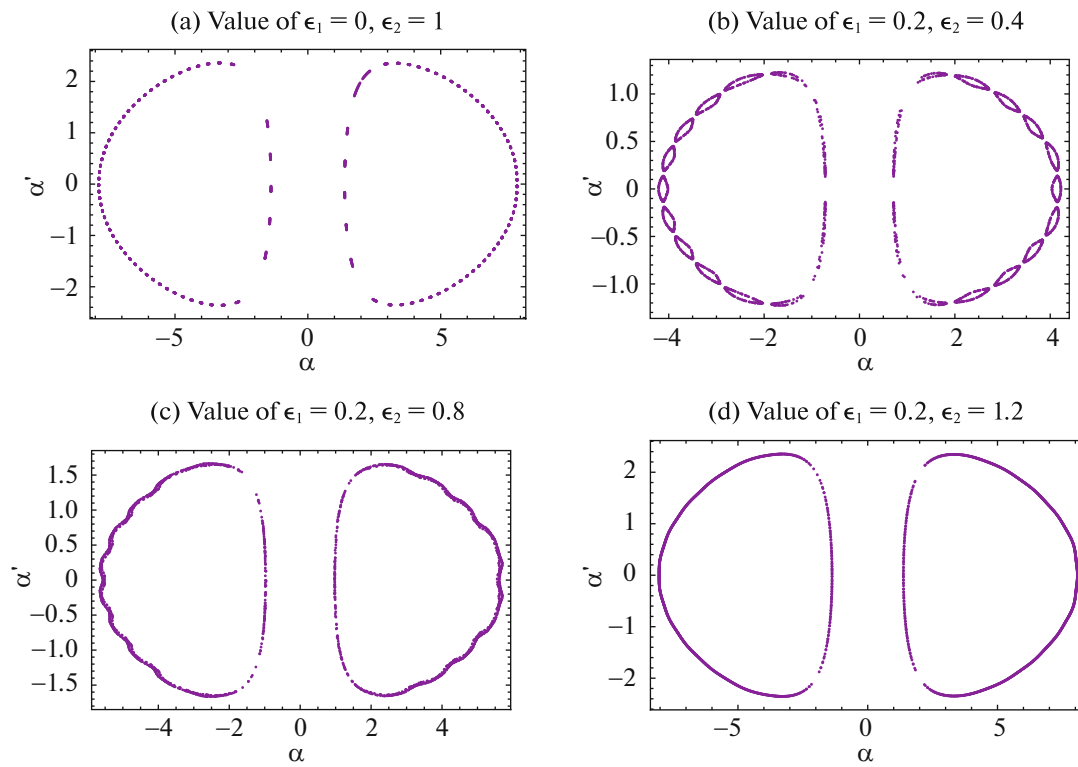


Fig. 4. Poincaré surfaces of section in  $\alpha-\alpha'$ -plane at  $f = 0, e = 0.15, a = 0.75, \mu = 0.1, q = 0.9, A_2 = A_3 = 0.05$ .

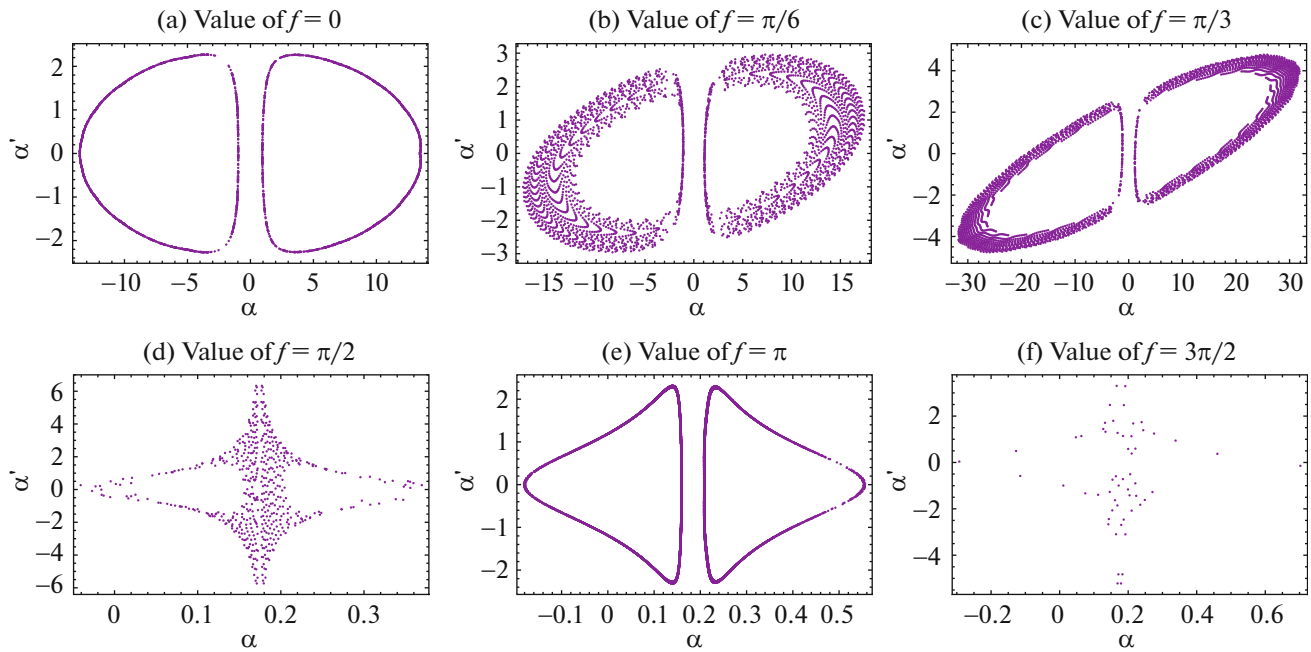


Fig. 5. Poincaré surfaces of section in  $\alpha-\alpha'$ -plane at  $\epsilon_1 = 0, \epsilon_2 = 1, e = 0.15, a = 0.75, \mu = 0.1, q = 0.9, A_2 = A_3 = 0.05$ .

region corresponding to the equilibrium points  $L_{3,4}$  and shows that the small particle can move only near the three primaries  $m_1, m_2,$  and  $m_3$  in circular regions where  $L_3$  and  $L_4$  are gateway for the regions near  $m_2$  and  $m_3$  and it can not move in purple shaded region

i.e., near the equilibrium points  $L_2, L_5, L_6, L_7,$  and  $L_8$ . Figure 8d represents the region corresponding to the equilibrium points  $L_5, L_6$  and shows that the small particle can move freely near the primaries while it can not move near the equilibrium points  $L_2, L_7,$

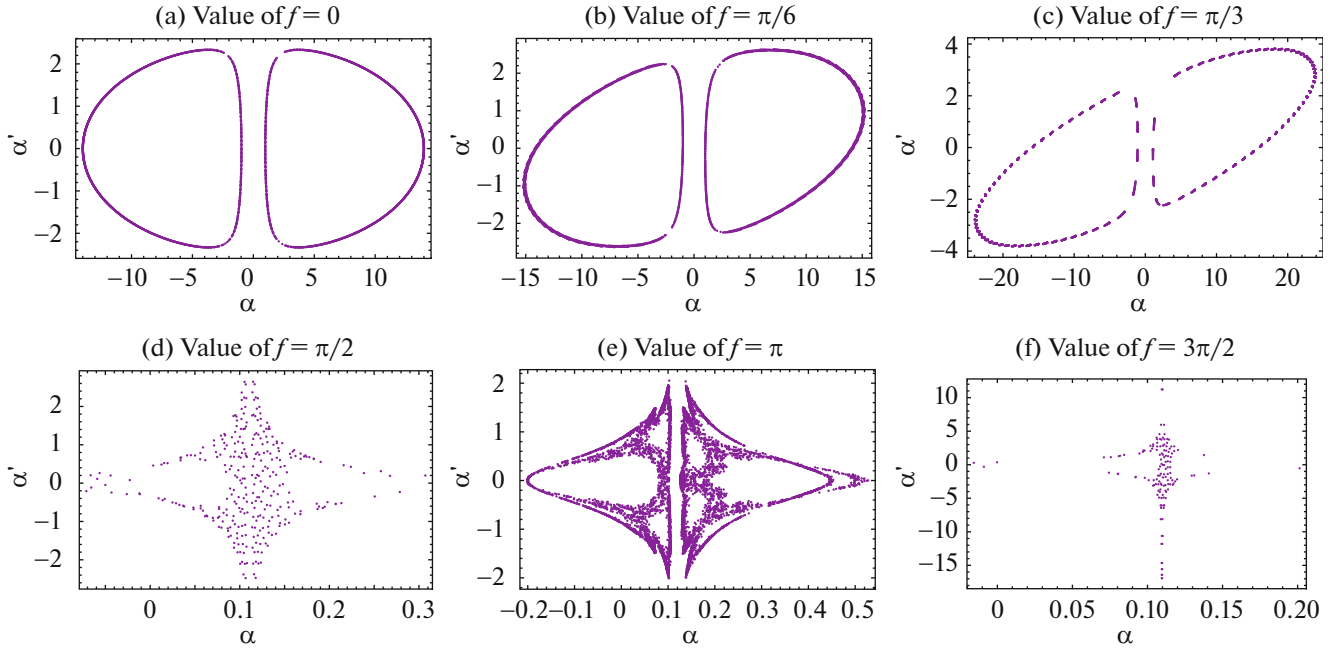


Fig. 6. Poincaré surfaces of section in  $\alpha-\alpha'$ -plane at  $\epsilon_1 = 0.2, \epsilon_2 = 0.4, e = 0.15, a = 0.75, \mu = 0.1, q = 0.9, A_2 = A_3 = 0.05$ .

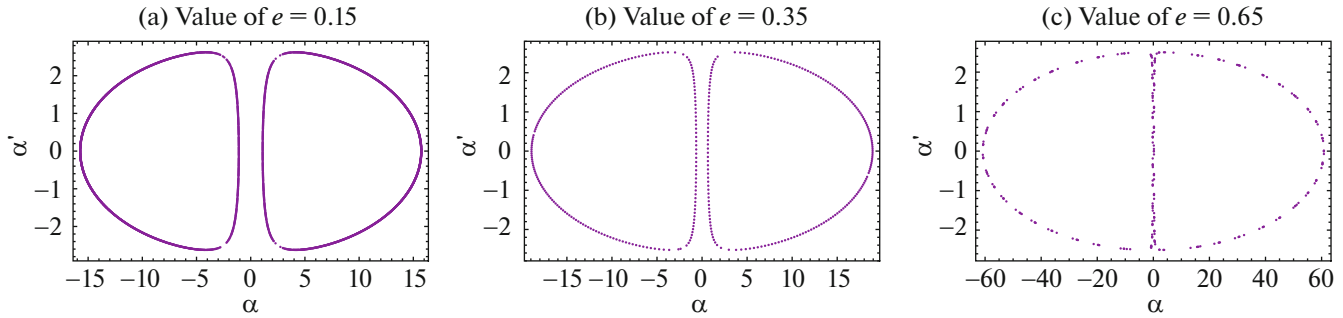


Fig. 7. Poincaré surfaces of section in  $\alpha-\alpha'$ -plane at  $f = 0, \epsilon_1 = 0.2, \epsilon_2 = 0.4, a = 0.75, \mu = 0.1, q = 0.9, A_2 = A_3 = 0.05$ .

and  $L_8$ . Figure 8e represents the region corresponding to the equilibrium points  $L_7, L_8$  and shows that the small particle can move freely except near the equilibrium points  $L_2, L_7$ , and  $L_8$ . Black points are showing the positions of the equilibrium points while red circles and star are presenting the locations of the primaries.

### 3.4. Basins of Attracting Domain

To reveal the basins of attractive domain for the infinitesimal body, we use very simple iterative method known as Newton–Raphson iterative method. The attracting domains which are the most important qualitative behaviour of the dynamical systems and are composed by all the initial values that tend to a

specific attracting point which is one of the equilibrium points. Using the above iterative method, we have illustrated the attracting domain in  $\alpha-\beta$ -plane for the parameters used. The algorithm of the problem is given as:

$$\alpha_{n+1} = \alpha_n - \left( \frac{U_\alpha U_{\beta\beta} - U_\beta U_{\alpha\beta}}{U_{\alpha\alpha} U_{\beta\beta} - U_{\alpha\beta} U_{\beta\alpha}} \right)_{(\alpha_n, \beta_n)}, \quad (10)$$

$$\beta_{n+1} = \beta_n - \left( \frac{U_\beta U_{\alpha\alpha} - U_\alpha U_{\beta\alpha}}{U_{\alpha\alpha} U_{\beta\beta} - U_{\alpha\beta} U_{\beta\alpha}} \right)_{(\alpha_n, \beta_n)}, \quad (11)$$

where  $\alpha_n, \beta_n$  are the values of  $\alpha$  and  $\beta$  coordinates of the  $n$ th step of the Newton–Raphson iterative process. If the initial point converges rapidly to one of the equilibrium points then this point  $(\alpha, \beta)$  will be a member of the attracting domain. This process

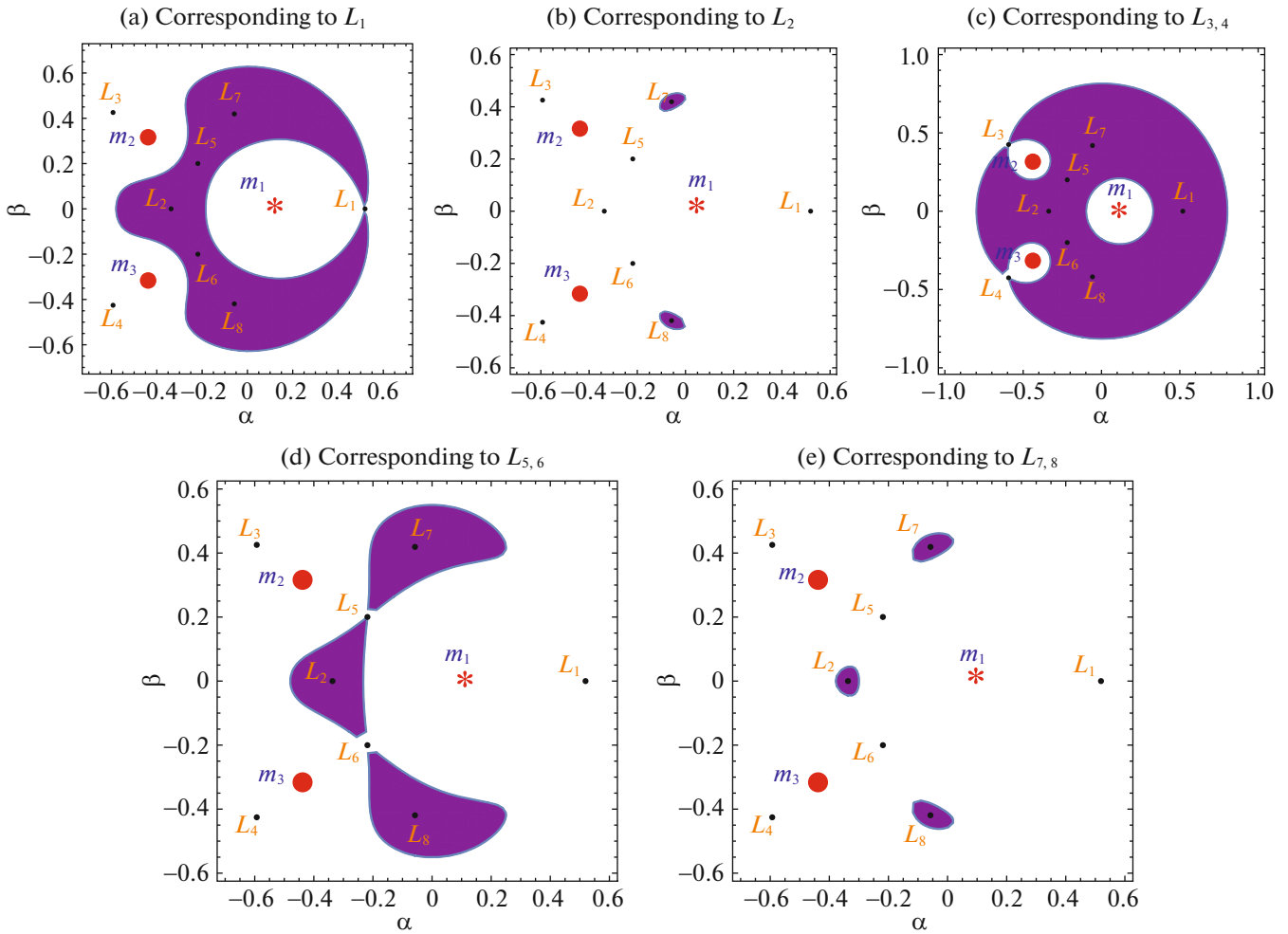


Fig. 8. Regions of possible motion in  $\alpha$ - $\beta$ -plane at  $\epsilon_1 = 0.2$ ,  $\epsilon_2 = 0.4$ ,  $f = 0$ ,  $a = 0.75$ ,  $\mu = 0.1$ ,  $q = 0.9$ ,  $A_2 = A_3 = 0.05$ .

stops when the successive approximation converges to an equilibrium point. We also need to clear that the attracting domain is not related with the classical attracting domain in dissipative system. For the classification of different equilibrium points on the plane, we used a color code. We have plotted the attracting domain for eccentricity  $e = -0.15$  in  $\alpha$ - $\beta$ -plane and given in Fig. 9a. Figure 9b represents the zoomed part of Fig. 9a near the configuration of the primaries, from here we observed that there are eight attracting points  $L_1, L_2, L_3, L_4, L_5, L_6, L_7$ , and  $L_8$ . From the Fig. 9b, we found that  $L_1, L_2$  corresponds to the light blue color region,  $L_3, L_5$  corresponds to the red color region,  $L_4, L_8$  corresponds to the yellow color region,  $L_5$  corresponds to the blue color region and  $L_6$  corresponds to the green color region, all these regions extended to infinity.

Also we have plotted the attracting domain for  $e = 0.65$  in  $\alpha$ - $\beta$ -plane and given in Fig. 9c. The zoomed part of Fig. 9c is Fig. 9d, we found four attracting points  $L_1, L_2, L_3$ , and  $L_4$ . We observed from this

figure that  $L_1, L_2$  corresponds to the light green color regions which is extended to infinity,  $L_3$  corresponds to the blue color region,  $L_4$  correspond to the green color region, all these regions are extended to infinity. In all the figures black dots are representing the locations of the attracting points.

#### 4. STABILITY OF EQUILIBRIUM POINTS

To reveal the stability of equilibrium points of the infinitesimal variable mass in its vicinity  $(\alpha_0 + \alpha_1, \beta_0 + \beta_1)$  under the effect of the oblate radiating primaries. Where  $(\alpha_1, \beta_1)$  are small displacements from the equilibrium points  $(\alpha_0, \beta_0)$ .

In the phase space, the system (4) can be rewritten as

$$\begin{aligned} \alpha'_1 &= \epsilon_3 \alpha_2, \\ \beta'_1 &= \epsilon_3 \beta_2, \\ \alpha'_2 &= -\frac{\epsilon_4}{\epsilon_3} \alpha_2 + 2\beta_2 + \frac{U_{\alpha\alpha}^0}{\epsilon_3} \alpha_1 + \frac{U_{\alpha\beta}^0}{\epsilon_3} \beta_1, \end{aligned}$$



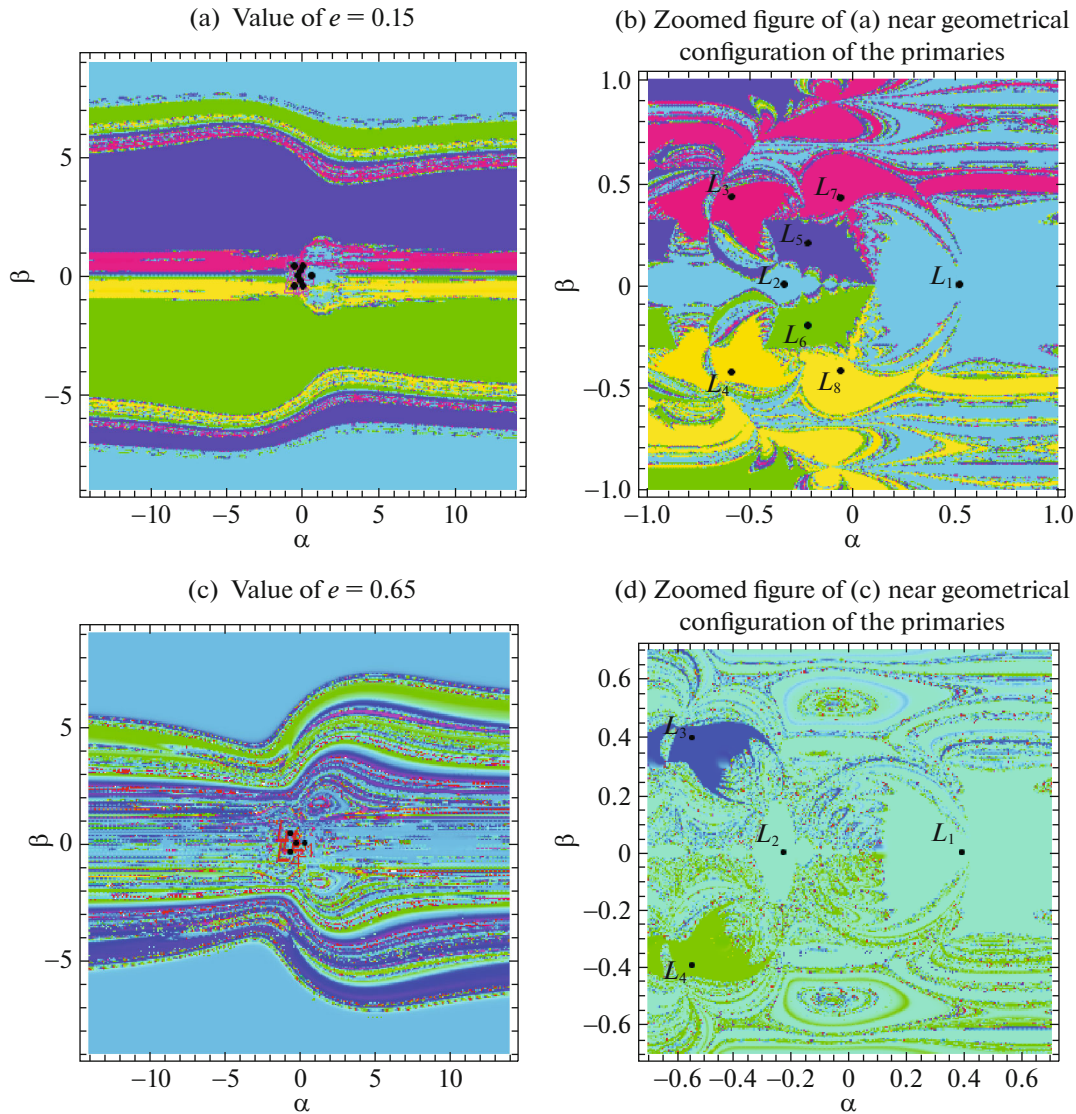


Fig. 9. Basins of Attracting domain in  $\alpha$ - $\beta$ -plane at  $\epsilon_1 = 0.2, f = 0, a = 0.75, \epsilon_2 = 0.4, \mu = 0.1, q = 0.9, A_2 = A_3 = 0.05$ .

$$\beta'_2 = -\frac{\epsilon_4}{\epsilon_3}\beta_2 - 2\alpha_2 + \frac{U^0_{\beta\alpha}}{\epsilon_3}\alpha_1 + \frac{U^0_{\beta\beta}}{\epsilon_3}\beta_1, \quad (12)$$

where the superscript 0 denotes the value at the corresponding equilibrium point.

Due to variation in the mass and distance of the small particle, we use Meshcherskii space-time inverse transformations to examine the stability of the equilibrium points.

$$\begin{aligned} \alpha_3 &= \epsilon_2^{-1/2}\alpha_1, & \beta_3 &= \epsilon_2^{-1/2}\beta_1, \\ \alpha_4 &= \epsilon_2^{-1/2}\alpha_2, & \beta_4 &= \epsilon_2^{-1/2}\beta_2. \end{aligned} \quad (13)$$

With the help of Eq. (12), the system (13) can be written as follows:

$$\mathbf{Z}' = M \mathbf{Z}, \quad (14)$$

where

$$\mathbf{Z}' = \begin{pmatrix} \alpha'_3 \\ \beta'_3 \\ \alpha'_4 \\ \beta'_4 \end{pmatrix}, \quad \mathbf{Z} = \begin{pmatrix} \alpha_3 \\ \beta_3 \\ \alpha_4 \\ \beta_4 \end{pmatrix} \quad (15)$$

and

$$M = \begin{pmatrix} \frac{1}{2}\epsilon_1 & 0 & \epsilon_3 & 0 \\ 0 & \frac{1}{2}\epsilon_1 & 0 & \epsilon_3 \\ \frac{U^0_{\alpha\alpha}}{\epsilon_3} & \frac{U^0_{\alpha\beta}}{\epsilon_3} & \left(\frac{\epsilon_1}{2} - \frac{\epsilon_4}{\epsilon_3}\right) & 2 \\ \frac{U^0_{\beta\alpha}}{\epsilon_3} & \frac{U^0_{\beta\beta}}{\epsilon_3} & -2 & \left(\frac{\epsilon_1}{2} - \frac{\epsilon_4}{\epsilon_3}\right) \end{pmatrix}. \quad (16)$$

**Table 1.** The nature of equilibrium points at  $f = 0, q = 0.9, A_2 = A_3 = 0.05, a = 0.75, \mu = 0.1, \epsilon_1 = 0.2, \epsilon_2 = 0.4$ 

Equilibrium point			Roots	Nature
$e$	$\alpha$ -Co	$\beta$ -Co		
0.15	0.5192068365	0.0000000000	$0.1000000000 \pm 1.2555742261i$ $0.7353184364$ $-0.5353184364$	Unstable
	-0.3368997735	0.0000000000	$-0.7818462262 \pm 0.9956472643i$ $0.9818462262 \pm 0.9956472643i$	Unstable
	-0.5931143451	$\pm 0.4255075646$	$0.0999999999 \pm 1.7235222930i$ $\pm 2.5697014680$	Unstable
	-0.0577875673	$\pm 0.4191556178$	$-0.4090586590 \pm 0.9215456777i$ $0.6090586590 \pm 0.9215456777i$	Unstable
	-0.2187095570	$\pm 0.2002343086$	$0.1000000000 \pm 1.5530836905i$ $1.8751301053$ $-1.6751301053$	Unstable
0.35	0.4836445044	0.0000000000	$0.0999999999 \pm 1.3618577961i$ $-0.4314916798$ $0.6314916798$	Unstable
	-0.3045934436	0.0000000000	$-0.4704939751 \pm 0.9731132762i$ $0.6704939751 \pm 0.9731132762i$	Unstable
	-0.5795768410	$\pm 0.4164988058$	$0.1000000000 \pm 1.7170447754i$ $-2.2936977578$ $2.4936977578$	Unstable
	-0.0862030276	$\pm 0.3629651023$	$-0.1649224210 \pm 0.9186656773i$ $0.3649224210 \pm 0.9186656773i$	Unstable
	-0.2003803512	$\pm 0.2086528558$	$0.1000000000 \pm 1.3922596495i$ $1.2321348043$ $-1.0321348043$	Unstable
0.65	0.3905452636	0.0000000000	$0.1000000000 \pm 1.4789916747i$ $-0.3858539748$ $0.5858539748$	Unstable
	-0.2267764684	0.0000000000	$0.1000000000 \pm 0.4687643427i$ $0.0999999999 \pm 1.3908705028i$	Unstable
	-0.5472692772	$\pm 0.3943513985$	$0.1000000000 \pm 1.7990658690i$ $-2.5146826257$ $2.7146826257$	Unstable

**Table 2.** The nature of equilibrium points at  $f = 0, q = 0.9, A_2 = A_3 = 0.05, a = 0.75, \mu = 0.1, \epsilon_1 = 0.2, e = 0.15$

Equilibrium point			Roots	Nature
$\epsilon_2$	$\alpha$ -Co	$\beta$ -Co		
0.80	0.7329068365	0.0000000000	$0.1000000000 \pm 1.2584428959i$ 0.7469110225 -0.5469110225	Unstable
	-0.4764482288	0.0000000000	$-0.7818462262 \pm 0.9956472643i$ $0.981846226292 \pm 0.9956472643i$	
	-0.3093020217	$\pm 0.2831740749$	$0.0999999999 \pm 1.5530836905i$ 1.8751301053 -1.6751301053	Unstable
	-0.8387903508	$\pm 0.6017585688$	$0.1000000000 \pm 1.7235222930i$ 2.5697014680 -2.3697014680	
	-0.0817239615	$\pm 0.5927755594$	$-0.4090586590 \pm 0.9215456777i$ $0.6090586590 \pm 0.9215456777i$	Unstable
	1.2	0.9136445044	0.0000000000	
-0.5835275247		0.0000000000	$-0.7181530525 \pm 0.9688286891i$ $0.9181530525 \pm 0.9688286891i$	Unstable
-0.3788160648		$\pm 0.3468159960$	$0.1000000000 \pm 1.9508653141i$ -2.7831628987 2.9831628987	
-1.0273041804		$\pm 0.7370007209$	$-0.0587092569 \pm 0.9543910748i$ $0.2587092569 \pm 0.9543910748i$	Unstable
-0.1000910027		$\pm 0.7259988263$	$-0.3130124638 \pm 0.9793242943i$ $0.5130124638 \pm 0.979324294307i$	

The characteristic equation for the matrix  $M$  is

$$\lambda^4 + B_3\lambda^3 + B_2\lambda^2 + B_1\lambda + B_0 = 0, \quad (17)$$

where

$$B_0 = \frac{1}{16}\epsilon_1^4 + \frac{1}{4}\epsilon_1^2 \left( 4 - U_{\alpha\alpha} - U_{\beta\beta} + \frac{\epsilon_4^2}{\epsilon_3^2} - \frac{\epsilon_1\epsilon_4}{\epsilon_3} \right) + (U_{\alpha\alpha}U_{\beta\beta} - U_{\alpha\beta}^2) + \frac{\epsilon_1\epsilon_4}{2\epsilon_3}(U_{\alpha\alpha} + U_{\beta\beta}),$$

$$B_1 = \epsilon_1 \left( -4 + U_{\alpha\alpha} + U_{\beta\beta} - \frac{\epsilon_1^2}{2} + \frac{3\epsilon_1\epsilon_4}{2\epsilon_3} - \frac{\epsilon_4^2}{\epsilon_3^2} \right) - \frac{\epsilon_4}{\epsilon_3}(U_{\alpha\alpha} + U_{\beta\beta}),$$

$$B_2 = 4 - U_{\alpha\alpha} - U_{\beta\beta} + \frac{3\epsilon_1^2}{2} - \frac{3\epsilon_1\epsilon_4}{\epsilon_3} + \frac{\epsilon_4^2}{\epsilon_3^2},$$

$$B_3 = -2\epsilon_1 + \frac{2\epsilon_4}{\epsilon_3}. \quad (18)$$

**Table 3.** The nature of equilibrium points at  $f = 0, e = 0.15, A_2 = A_3 = 0.05, a = 0.75, \mu = 0.1, \epsilon_1 = 0.2, \epsilon_2 = 0.4$

Equilibrium point			Roots	Nature
$q$	$\alpha$ -Co	$\beta$ -Co		
0.5	0.4428325638	0.0000000000	$0.1000000000 \pm 1.2683314085i$ 0.7894415203 -0.5894415203	Unstable
	-0.2505255446	0.0000000000	$-0.6150858991 \pm 0.9298592577i$ 0.8150858991 $\pm 0.9298592577i$	Unstable
	-0.1707503483	$\pm 0.1836823541$	$0.1000000000 \pm 1.3180544970i$ 1.2828821336 -1.0828821336	Unstable
	-0.5898644151	$\pm 0.4213054143$	$0.1000000000 \pm 1.7919781496i$ 2.7367106283 -2.5367106283	Unstable
	-0.0437661060	$\pm 0.3338939695$	$-0.3675802800 \pm 0.8913827867i$ 0.5675802800 $\pm 0.8913827867i$	Unstable
	0.70	0.4856445044	0.0000000000	$0.0999999999 \pm 1.2597605252i$ -0.5538417703 0.7538417703
-0.2958676114		0.0000000000	$-0.7191993843 \pm 0.9731331379i$ 0.9191993843 $\pm 0.9731331379i$	Unstable
-0.1988983404		$\pm 0.1924567432$	$0.0999999999 \pm 1.4362377527i$ -1.3925152111 1.5925152111	Unstable
-0.5914732499		$\pm 0.4233460490$	$0.1000000000 \pm 1.7574615139i$ -2.4529832784 2.6529832784	Unstable
-0.0487667986		$\pm 0.3818961192$	$-0.3972280056 \pm 0.9123511370i$ 0.5972280056 $\pm 0.9123511370i$	Unstable

After numerically solving Eq. (17) for the different values of parameters used and evaluated the characteristic roots corresponding to each equilibrium points which are given in Tables 1–4. From these tables we concluded that all the equilibrium points are unstable because at-least one characteristic root

is either positive real number or positive real part of the complex characteristic root. While Dewangan et al. (2020) have shown that all equilibrium points are stable without variable of mass. Therefore, the variation parameters have great impact on the stability of equilibrium points.

**Table 4.** The nature of equilibrium points at  $f = 0, e = 0.15, q = 0.9, a = 0.75, \mu = 0.1, \epsilon_1 = 0.2, \epsilon_2 = 0.4$

Equilibrium point			Roots	Nature
$A_1 = A_2$	$\alpha$ -Co	$\beta$ -Co		
0.0	0.5404586875	0.0000000000	$0.0999999999 \pm 1.2514476805i$ 0.7169888788 -0.5169888788	Unstable
	-0.3668278224	0.0000000000	$-0.6708729108 \pm 0.9955344712i$ 0.8708729108 $\pm 0.9955344712i$	
	-0.2403690612	$\pm 0.2117754044$	$0.0999999999 \pm 1.6038997602i$ 1.7292039542 -1.5292039542	Unstable
	-0.5679802751	$\pm 0.4076186271$	$0.1000000000 \pm 1.8821740449i$ 2.1992822307 -1.9992822307	
	-0.0685298470	$\pm 0.4396918348$	$-0.3595884008 \pm 0.9153677703i$ 0.5595884008 $\pm 0.9153677703i$	Unstable
	0.10	0.5014059128	0.0000000000	
-0.3134559329	0.0000000000	$-0.8315979025 \pm 0.9918988849i$ 1.0315979025 $\pm 0.9918988849i$	Unstable	
-0.2041890691	$\pm 0.1935248093$	$0.1000000000 \pm 1.5091344970i$ -1.6712553549 1.8712553549		Unstable
-0.6030521443	$\pm 0.4326318450$	$0.0999999999 \pm 1.6851964874i$ -2.4786922935 2.6786922935	Unstable	
-0.0508327967	$\pm 0.4011246287$	$-0.4392166036 \pm 0.9238817029i$ 0.6392166036 $\pm 0.9238817029i$		Unstable

5. CONCLUSIONS

The effects of generalized parameters are studied in the restricted elliptic four-body problem where infinitesimal body varies its mass according to Jean's law and one of the primaries is radiating as well as another two are oblate in shapes. The equations of

motion are evaluated by using Meshcherskii-space time transformations where the variation parameters ( $\epsilon_1$  and  $\epsilon_2$ ) are clearly visible with excellent role for this problem. We numerically studied as well as plotted the equilibrium points, Poincaré surfaces of section, regions of possible motion and basins of attracting

domain with the variation of parameters used. Here at most eight equilibrium points are found, out of which two are collinear ( $L_1$  and  $L_2$ ) and other six are non-collinear ( $L_3$ ,  $L_4$ ,  $L_5$ ,  $L_6$ ,  $L_7$ , and  $L_8$ ) (Figs. 1–3). To study the dynamical behaviour of the infinitesimal body, we have plotted the Poincaré surfaces of section and found most of the cases regular while in some cases chaotic (Figs. 4–7). Further we have evaluated the value of Jacobi-constant corresponding to each equilibrium points and drawn the prohibited and allowed regions. In this case the purple shaded regions are the forbidden regions (Fig. 8). Further more we have drawn the basins of attracting domain for the variation of eccentricity of the elliptic path of the primaries and shown in Fig. 9. The different attracting domains present different color regions. Finally we examined the stability of equilibrium points numerically. The numerical values are given in the Tables 1–4. These tables represent the roots of the characteristic polynomial which show that at least one of the roots having either positive real part of the complex roots or only positive real root, which confirm that all the equilibrium points are unstable. This result is different from the result obtained by Dewangan et al. (2020), where they have shown that all the equilibrium points are stable. Therefore these variation parameters have great impact on the dynamical behaviour of the motion of the infinitesimal body.

#### REFERENCES

1. E. I. Abouelmagd and A. A. Ansari, *New Astron.* **73**, 101282 (2019).  
<https://doi.org/10.1016/j.newast.2019.101282>
2. E. I. Abouelmagd and A. Mostafa, *Astrophys. Space Sci.* **357**, 58 (2015).  
<https://doi.org/10.1007/s10509-015-2294-7>
3. A. A. Ansari, *Ital. J. Pure Appl. Math.* **38**, 581 (2017a).
4. A. A. Ansari, *Appl. Math. Nonlin. Sci.* **2**, 529 (2017b).
5. A. A. Ansari, *Appl. Appl. Math.: Int. J.* **13**, 818 (2018).
6. A. A. Ansari, Z. A. Alhussain, and P. Sadanand, *J. Astrophys. Astron.* **39**, 57 (2018).
7. A. A. Ansari, J. Singh, Z. Alhussain, and H. Belmabrouk, *New Astron.* **73**, 101280 (2019a).  
<https://doi.org/10.1016/j.newast.2019.101280>
8. A. A. Ansari et al., *J. Taibah Univ. Sci.* **13**, 670 (2019b).
9. A. A. Ansari et al., *Punjab Univ. J. Math.* **51** (5), 107 (2019c).
10. A. A. Ansari, A. Ali, M. Alam, and R. Kellil, *Appl. Appl. Math.: Int. J.* **14**, 985 (2019d).
11. A. Baltagiannis and K. E. Papadakis, *Int. J. Bifurcat. Chaos* **21**, 2179 (2011).  
[doi 10.1142/S0218127411029707](https://doi.org/10.1142/S0218127411029707)
12. A. Chakraborty and A. Narayan, *Few Body Syst.* **60** (7) (2019a).  
<https://doi.org/10.1007/s00601-018-1472>
13. A. Chakraborty and A. Narayan, *New Astron.* **70**, 43 (2019b).  
<https://doi.org/10.1016/j.newast.2019.02.002>
14. R. R. Dewangan, A. Chakraborty, and A. Narayan, *New Astron.* **78** (2020, in press).  
<https://doi.org/10.1016/j.newast.2020.101358>
15. C. N. Douskos, *Astrophys. Space Sci.* **326**, 263 (2010).
16. J. H. Jeans, *Astronomy and Cosmogony* (Cambridge Univ. Press, Cambridge, 1928).
17. T. J. Kalvouridis, *Astrophys. Space Sci.* **246**, 219 (1997).
18. R. Kumari and B. S. Kushvah, *Astrophys. Space Sci.* **344**, 347 (2013).
19. R. Kumari and B. S. Kushvah, *Astrophys. Space Sci.* **349**, 693 (2014).
20. L. G. Lukyanov, *Astron. Lett.* **35**, 349 (2009).
21. I. V. Meshcherskii, *Works on the Mechanics of Bodies of Variable Mass* (GITTL, Moscow, 1949) [in Russian].
22. R. K. Sharma and P. V. SubbaRao, *Celest. Mech.* **13**, 137 (1976). <http://dx.doi.org/10.1007/BF01232721>
23. J. Singh and B. Ishwar, *Celest. Mech.* **35**, 201 (1985).
24. J. Singh and A. E. Vincent, *British J. Math. Comput. Sci.* **19** (5), 1 (2016).
25. M. J. Zhang, C. Y. Zhao, and Y. Q. Xiong, *Astrophys. Space Sci.* **337**, 107 (2012). [doi 10.1007/s10509-011-0821-8](https://doi.org/10.1007/s10509-011-0821-8)
26. E. E. Zotos, *Astrophys. Space Sci.* **362** (2) (2017).